MULTI-SCALE CRYSTALLINE PLASTICITY FINITE ELEMENT ANALYSIS OF TEXTURE EVOLUTION IN DRAWING PROCESS

EIJI NAKAMACHI[1], TAKASHI YOSHIDA[1], HIROYUKI KURAMAE[2], TOSHIHIKO YAMAGUCHI[1], YUSUKE MORITA[1]

Abstract. The crystallographic control technology in the aluminum wire drawing process is a key technology in the aluminum industries, which produces high-strength bars and wires for the electric, automotive and aircraft parts. A newly proposed "process metallurgy" computational technology in the industrial forming process consists of the two-scale finite element (FE) analyses and the texture evolution prediction scheme. We developed two-scale FE analyses code based on the crystallographic homogenization method by considering the hierarchical structure of polycrystal aluminum material. It can be characterized as the combination of two-scale structure, such as the microscopic polycrystal structure and the macroscopic elastic plastic continuum. Micro polycrystal structure is modelled as a three dimensional representative volume element (RVE). RVE is featured as 3×3×3 (totally 27) eight-nodes solid finite elements, which has totally 216 crystal orientations. This FE analyses code can predict the deformation, strain and stress evolutions in the wire drawing processes in the macro-scale, and simultaneously the crystal texture and hardening evolutions in the micro-scale. In this study, we analyzed the texture evolution in the "three passes" wire drawing processes under conditions of specified drawing angles of die. We evaluated the texture evolution in the surface and center regions of the wire cross section, and to clarify the effects of processing conditions on the texture evolution.

Key words: two-scale analysis, Finite Element Method, optimum design, drawing process, texture evolution, crystal plasticity, process metallurgy.

1. INTRODUCTION

The aluminum alloy wire is used for the transmission line in the automotive industries from the viewpoint of weight reduction. However, the aluminum wire has a problem of low strength, even though its high conductivity. Until now, several trials have done to generate a high strength and high formability wire introducing the new concepts of material and process design. The main effort of these studies has been spent on the mechanical and material analyses at the macro-scale to detect the defects in the drawing process and design the die tool by

[1] Doshisha University, Kyotanabe, Kyoto, Japan, 610-0394, enakamac@mail.doshisha.ac.jp
[2] Osaka Institute of Technology, Osaka, Japan, 530-8568, hiroyuki.kuramae@oit.ac.jp

Ro. J. Techn. Sci. – Appl. Mechanics, Vol. 63, N° 2, P. 93–103, Bucharest, 2018

considering the lubrication and the conventional material. In recent years, the study of drawing process is devoted on the microstructure design of material, such as the crystallographic morphological design based on the crystal plasticity theory [1]. A specified texture with a preferred orientation, which is evolved in the drawing process, shows a high formability and high strength characteristics. Therefore, there occurred a very high demand to develop a fusion numerical technique of "process metallurgy simulation" by combining the multi-scale finite element (FE) analysis and the process optimization algorithm [2-5]. It can control the material property at the micro-scale - the crystal structure and the texture – through the drawing process optimization. Inakazu has reported that a particular drawn wire, which has a texture of {110} <111> orientation, shows a very high strength, by their enormous number of experimental observations [6]. However, a numerical technique to search the optimum crystallographic structure by considering the drawing process effect on the material properties has not been invented yet. In this study, we develop a fusion simulation technique – a process metallurgy analysis – combined with the two-scale finite element analysis and the texture evolution prediction analysis to design a new highly functionalized aluminum alloy.

2. TWO-SCALE ELASTIC/ PLASTIC FINTE ELEMENT METHOD

2.1. Macro- and micro-finite element methods

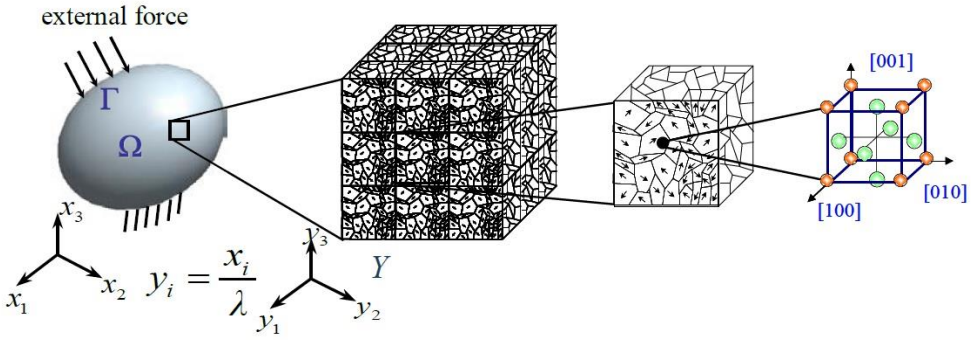

Fig. 1 – Macro continuum and micro polycrystal structures, and coordinates x_i and y_i.

Fig. 1 shows two-scale structures, such as a macro-continuum Ω and a micro-crystal structure Y. In the micro-structure, the RVE (representative volume element) consists of an polycrystal aggregation and is very small compared with the macro region Ω by a scale factor $\lambda << 1$. We introduce both microscopic and macroscopic coordinate systems so that physical quantities are represented by two different length scales; one is x in the macroscopic region Ω and the other is $y(=x/\lambda)$ in the microscopic region Y. Equations in the micro- and macroscopic

levels are derived by employing defined velocities, $\dot{U}_i$ and $\dot{u}_i$.

$$\dot{U}_i(x) = \dot{u}_i^0(x) : \text{in the macroscopic region,} \tag{1}$$

$$\dot{u}_i(x,y) = \frac{\partial \dot{u}_i^0(x)}{\partial x_j} y_j + \dot{u}_i^1(x,y) : \text{in the microscopic region.} \tag{2}$$

We assume that the perturbed velocity $\dot{u}_i^1$ equals to zero on the boundary of the micro crystal structure Y, such as $\dot{u}_i^1(x,y) = 0$, to satisfy the periodicity condition. The equation of virtual power principle for the micro polycrystalline structure is expressed as follows:

$$\begin{aligned} &\int_Y \rho \ddot{u}_i(x,y)\delta\dot{u}_i(x,y)\,\mathrm{d}Y + \int_Y \nu \dot{u}_i(x,y)\delta\dot{u}_i(x,y)\,\mathrm{d}Y = \\ &= -\int_Y \sigma_{ij}\delta\dot{u}_{i,j}(x,y)\,\mathrm{d}Y \end{aligned} \tag{3}$$

$$\delta\dot{u}_i(x,y) = 0 : \text{on the boundary of region } Y, \tag{4}$$

where ρ and ν are the mass density and the viscosity coefficient, respectively. By solving the governing equation, Eq. (4), we obtain the Cauchy stresses. The macroscopic Cauchy stress tensor, which means the homogenized stress tensor, is obtained by averaging Cauchy stresses in microstructure as follows:

$$\sigma_{ij}^H = \sum_{e=1}^{N_e}\left(\sum_{G=1}^{N_G}|J_G|\sigma_{ij}^G\right) \Big/ \sum_{e=1}^{N_e}|J_e| \tag{5}$$

where, σ_{ij}^G is Cauchy stress at Gaussian integration point (IP) *G* of a finite element in the microscopic region, $|J_G|$ is the Jacobian at the IP, N_G is the total number of IPs.

We introduced the homogenized stress σ_{ij}^H and formulate the virtual power equation of the macro continuum as follows:

$$\begin{aligned} &\int_\Omega \rho \ddot{U}_i(\boldsymbol{x})\delta\dot{U}_i(\boldsymbol{x})\,\mathrm{d}\Omega + \int_\Omega \nu \dot{U}_i(\boldsymbol{x})\delta\dot{U}_i(\boldsymbol{x})\,\mathrm{d}\Omega \\ &= \int_\Omega \overline{f}_i\,\delta\dot{U}_i(\boldsymbol{x})\,\mathrm{d}\Omega + \int_{\Gamma_\sigma} \overline{T}_i\,\delta\dot{U}_i(\boldsymbol{x})\,\mathrm{d}\Gamma - \int_\Omega \sigma_{ij}^H(\boldsymbol{x})\frac{\partial\delta\dot{U}_i(\boldsymbol{x})}{\partial x_j}\,\mathrm{d}\Omega \end{aligned} \tag{6}$$

where Ω, Γ_σ, $\overline{f}_i$ and $\overline{T}_i$ are the volume, force boundary surface, the body force and the external surface force.

$$\mathbf{M}^1\ddot{\mathbf{u}} + \mathbf{C}^1\dot{\mathbf{u}} = -\mathbf{F}^1 : \text{for the micro structure} \tag{7}$$

$$\mathbf{M}^0\ddot{\mathbf{U}} + \mathbf{C}^0\dot{\mathbf{U}} = -\mathbf{F}^0 : \text{for the macro structure} \tag{8}$$

where **M** and **C** are the mass and damping matrices, **F** and **P** are the internal and external force vectors, **u** and **U** are the micro and macro displacement vectors, respectively.

The displacement vectors of the next time step for the micro and macro levels can be updated without solving simultaneous equations. In order to obtain the internal force vector **F**, the macroscopic stresses are calculated through homogenization procedure by using stresses at all Gaussian integration points of micro finite elements. Therefore, the most of the computation time is consumed in the homogenized stress evaluations in the micro-FE mesh.

2.2. Elastic/crystal plasticity constitutive law

The conventional elastic/crystalline viscoplastic constitutive equation is used in the micro-polycrystal structure in the finite element procedure [7-12].

$$\dot{\gamma}^{(\alpha)} = \dot{\gamma}_0^{(\alpha)} \left[\frac{\tau^{(\alpha)}}{g^{(\alpha)}} \right] \left[\left| \frac{\tau^{(\alpha)}}{g^{(\alpha)}} \right| \right]^{(1/m)-1} \tag{9}$$

$$g^{(\alpha)} = g^{(\alpha)}(\gamma) \tag{10}$$

$$\dot{g}^{(\alpha)} = \sum_{(\beta)} h_{\alpha\beta} \left| \dot{\gamma}^{(\beta)} \right|, \quad h_{\alpha\beta} = qh(\gamma) + (1-q)\, h(\gamma)\, \delta_{\alpha\beta} \tag{11}$$

$$h(\gamma) = h_0 n C \left\{ C\left(\gamma_0 + \gamma\right) \right\}^{n-1} \tag{12}$$

Here, $\dot{\gamma}^{(\alpha)}$ denotes the shear strain rate at the slip system (α), $\tau^{(\alpha)}$ the resolved shear stress(RSS), $g^{(\alpha)}$ the reference shear stress, $\dot{\gamma}_0^{(\alpha)}$ the reference shear strain rate and m the material rate sensitivity, $h_{\alpha\beta}$ the hardening coefficients, q_{ab} the self and latent hardening matrices, τ_0 the critical resolved shear stress (CRSS), h_0 the initial hardening ratio, n the strain hardening exponent and C the hardening coefficient.

The tangent modulus method is introduced for the stable time integration. Finally, Jaumann rate of Cauchy stress can be related to the rate of deformation D_{ij} as follows:

$$\hat{\sigma}_{ij}^{\lambda} = C_{ijkl}^{V\lambda} D_{kl}^{\lambda} - \sum_{(\alpha)} R_{ij}^{(\alpha)\lambda} \dot{f}^{(\alpha)\lambda} \tag{13}$$

3. TWO-SCALE FINITE ELEMENT MODEL FOR DRAWING PROCESS ANALYSES

We constructed FE models for the texture evolution analyses of the drawing process of the pure aluminum A1050. The crystal orientations measured by SEM-EBSD were introduced into integration points of the micro-finite elements of the representative volume element (RVE). We measured the crystal orientation distribution on the surface by using SEM-EBSD as shown in Fig. 2a and searched a minimum number of crystal orientations (grains) to represent the crystal plasticity constitutive law, which satisfied both the periodicity of crystallographic morphology and constitutive law. Finally we found that 216 crystal orientations were enough for RVE – 3×3×3 micro finite elements, totally 27 elements. Figure 2b shows the crystal orientation distributions of RVEs – {111} pole figure.

Three crystal material parameters, τ_0, h_0 and n, of the hardening evolution equation (12) were identified by the least square method using FE analyses results of the uni-axial tension tests through the comparison with the experimental results. Figure 3 shows stress-strain curves obtained by the experiments of tensile test in the drawing direction (DD) and the multi-scale FE results by employing 27 (=3×3×3) micro FEs with 216 Gaussian integration points. Table 2 summarizes identified crystal plastic material properties.

4. RESULTS AND DISCUSSION

4.1. Material parameter identification of constitutive laws

Parameter identification method and results of temperature-dependent constitutive equations of elasto-plasticity and crystal plasticity are shown. A true stress-true strain diagram obtained by a uniaxial tensile test at each temperature of Nakanishi et al. (12) was used for identification. Curve fitting was performed, and parameter identification was performed so that the sum of residual sum of squares at each temperature was minimized. Curve fitting in elasto-plasticity analysis and crystal plasticity analysis is shown in Fig. 3. The solid line is the analysis result, and the broken line is the experiment result of Nakanishi et al.

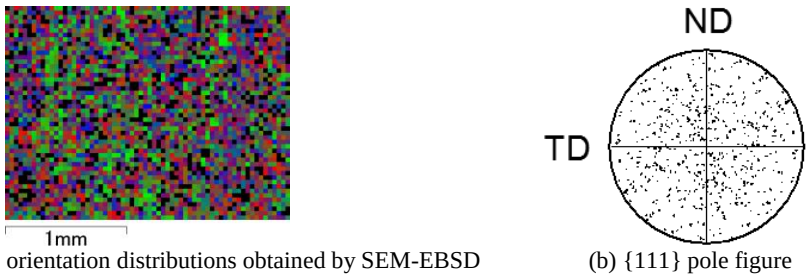

(a) Crystal orientation distributions obtained by SEM-EBSD (b) {111} pole figure

Fig. 2 – SEM-EBSD measurement results and {111} pole figure of the pure aluminum.

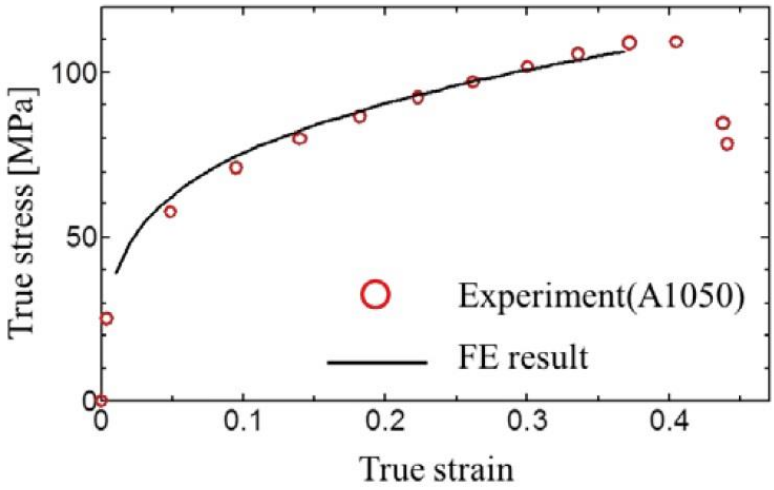

Fig. 3 – Stress-strain curves obtained by experiments and FE analyses using RVE-FE model.

Table 1
Material properties of crystal plasticity constitutive model

n		0.1
τ_0	[MPa]	4
h_0	[MPa]	24

4.2. Finite element models and die tool models

The wire drawing process of diameter reduction was performed by three conical die passes. We analyzed tree-passes by using the conical dies as shown in Fig. 4a to investigate the texture evolution at each drawing process. Fig. 4a shows a wire FE models, which diameter is 10 mm and the initial length is 80 mm. Its

macro-continuum FE model employed 8-node iso-parametric solid element, and a total number of finite elements was 1620. We have modeled so as to enter smoothly into the conical die by using initially squeezed edge as shown in Fig.4a. The micro- FE model - RVE polycrystal model – was divided into 27 (= 3×3×3) 8-node solid elements with 216 crystal orientations. We employed the enforced displacement in the drawing direction (DD) at the tip of the round wire. We employed the conical die angle as shown in Fig.4a such as 6 deg, to design the reduction in area as 20%. Diameters of die edge were different as shown in Fig.4b. The coefficient of friction between the die and wire was set as 0.02.

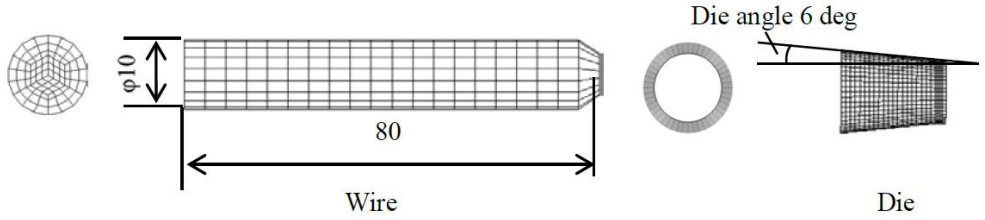

(a) FE models and three conical die models for three-passes drawing process

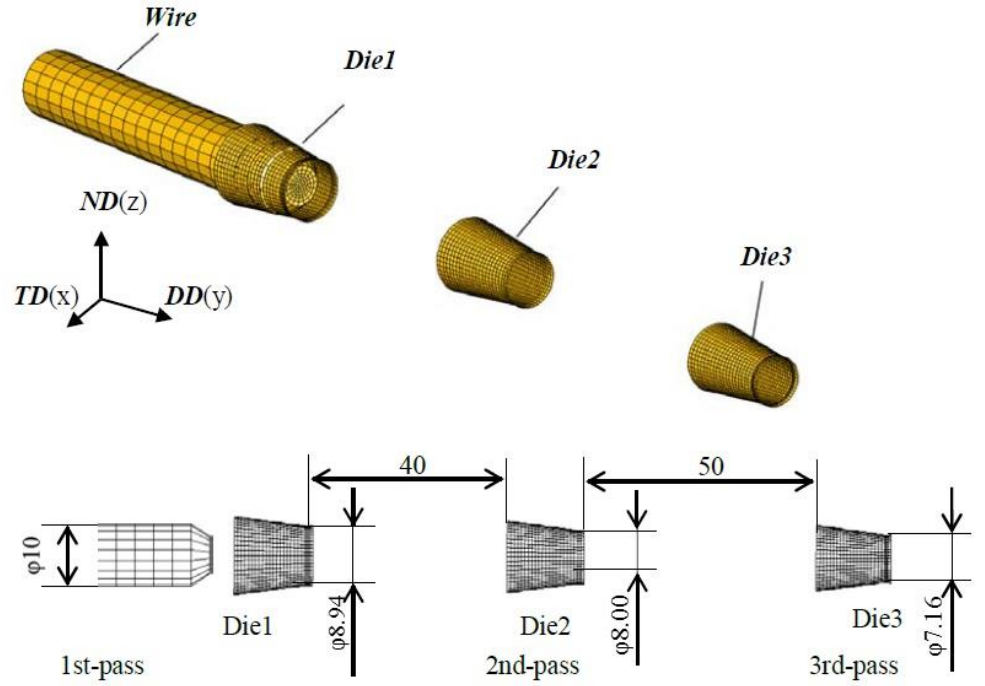

(b) Die set up for three passes wire drawing process

Fig. 4 – Macro-FE models of the wire and three conical dies for the wire drawing process simulation.

4.3. Crystal plastic plasticity exothermal analysis

We carried out two-scale FE analyses of the three passes wire drawing process. Fig. 5 shows deformed meshes obtained by macro-FE analyses and comparisons of shear strain distributions of wire FE models at three passes. Fig. 5 shows the axial-radial sectional views of shear strain distributions at three passes, because of the axisymmetric deformation. It was confirmed that the closer to the surface the higher the shear strain, and further the more the number of drawing pass the larger the strain.

Fig. 6 shows comparisons of the strain paths of the surface region and the center region, which correspond to the described macro finite elements, marked by the red color circle as shown in Fig. 6. The vertical axis shows the shear strain and the horizontal one the tensile strain in the drawing direction. It was confirmed that the shear strain increased drastically in the surface region and the tensile strain was dominated in both the surface and center regions. The strain increased rapidly at the first and second passes according to the combination effect of the cross sectional reduction and hardening evolution.

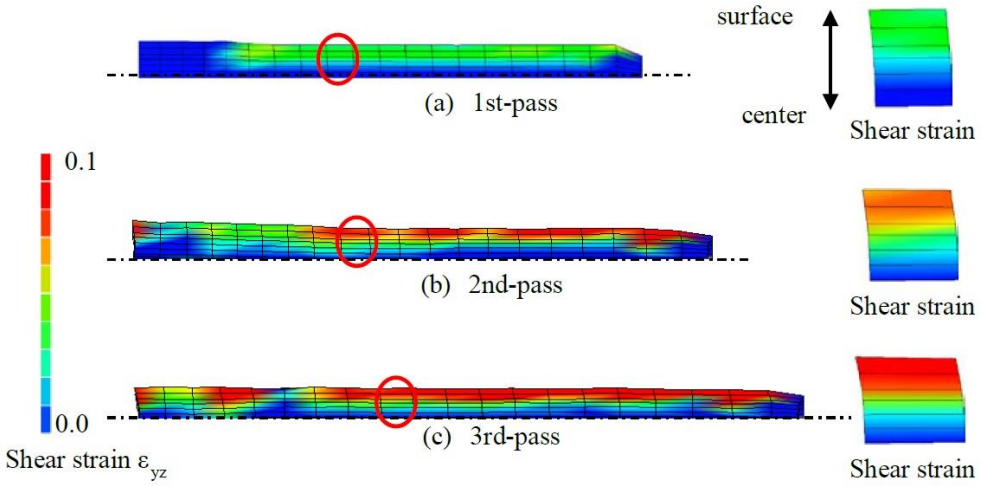

Fig. 5 – deformed shapes of macro-FE models with shear strain.

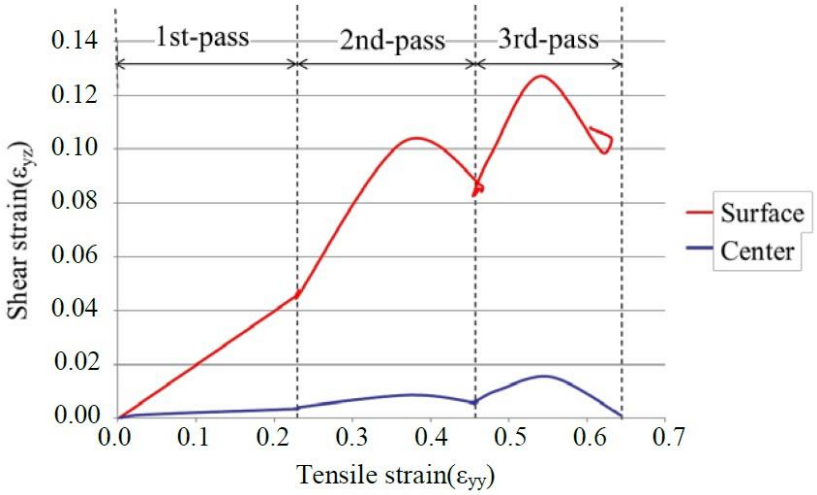

Fig. 6 – Strain strain paths of FEs of the surface and the center regions.

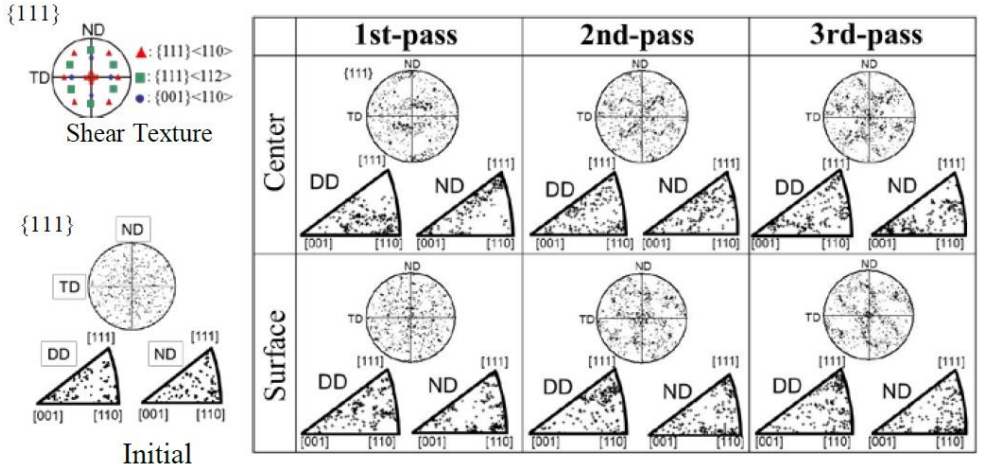

Fig. 7 – Texture evolutions at each pass of drawing by employing {111} pole figure and the inverse pole figure.

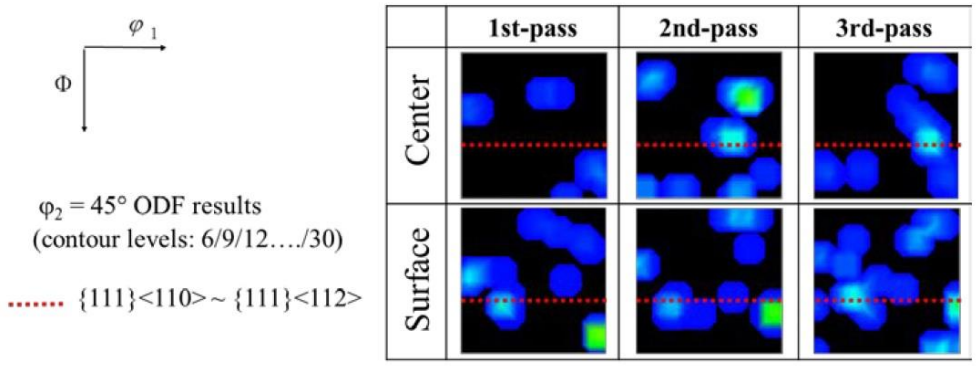

Fig. 8 – ODF results of orientation contours at $\varphi_2 = 45$ deg. plane at 1st, 2nd and 3rd passes.

Fig. 7 shows {111} pole figures and the inverse pole figures to compare the texture evolutions at 1st, 2nd and 3rd passes. We confirmed that the more the pass, the more the concentration toward {111} orientation. Further, it was demonstrated that the region closer to the surface, the more the concentration toward {111} orientation was found. On the other hand, we observed the double texture structure, {111} and {100} orientations in the center region, which is the typical texture of FCC metal by drawing process. Fig. 8 shows ODF results of orientation contours at $\varphi_2 = 45$ deg. plane at 1st, 2nd and 3rd passes to compare the texture evolution at the surface and center regions. The similar results with the pole figures as shown in Fig. 7 were obtained.

5. CONCLUSION

Numerical results of two-scale FE analyses of three passes wire drawing process show clearly the strain evolution at the macro-scale and the texture evolution at the micro-scale. It suggests that our two-scale analyses could predict the texture evolution, as summarized below:

1. The shear strain increases in the surface region and the tensile strain is dominated in both the surface and center regions.
2. The more the pass, the more the concentration toward {111} orientation in the surface region is observed. The double texture structure, {111} and {100} orientations, was found in the center region, which is the typical texture of FCC metal by drawing process.

In the future, our two-scale FE analyses of multi-passes wire drawing process will be a powerful tool to design the micro crystallographic structure of wire, by confirming the strength of wire using the conventional FE analysis code.

Received on December 25, 2017

REFERENCES

1. CHEN, J., YAN, W., LIU, C.X., DING, R.G., FAN, X.H., *Dependence of texture evolution on initial orientation in drawn single crystal copper*, Mater. Charact., **62**, *2*, pp. 237-242, 2011.
2. NAKAMACHI, E., TAM, N.N., MORIMOTO, H., *Multi-scale finite element analyses of sheet materials by using SEM-EBSD measured crystallographic RVE models*, Int. J. Plasticity, **23**, *3*, pp. 450-489, 2007.
3. NAKAMACHI, E., XIE, C.L., MORIMOTO, H., MORITA, K., YOKOYAMA, N., *Formability assessment of FCC aluminum alloy sheet by using elastic/crystalline viscoplastic finite element analysis*, Int. J. Plasticity, **18**, *5-6*, pp. 617-632, 2002.
4. NAKAMACHI, E., HIRAIWA, K., MORIMOTO, H., HARIMOTO, M., *Elastic/crystalline viscoplastic finite element analyses of single- and poly-crystal sheet deformations and their experimental verification*, Int. J. Plasticity, **16**, *12*, pp. 1419-1441, 2000.
5. NAKAMACHI, E., DONG, X., *Study of texture effect on sheet failure in a limit dome height test by using elastic/crystalline viscoplastic finite element analysis*, J. App. Mech., **64**, *3*, pp. 519-524, 1997.
6. INAKAZU, N., *Drawing and fiber texture formation for aluminum*, J. JILM, **37**, pp. 381-393, 1987.
7. NEEDLEMAN, A., *Finite element for finite strain plasticity problems*, Proc. The Workshop on Plasticity of Materials at Finite Strain, pp. 1-11, 1981.
8. ASARO, R.J., *Crystal plasticity*, J. App. Mech., **50**, *4b*, pp. 921-934, 1983.
9. ASARO, R.J., NEEDLEMAN, A., *Texture development and strain hardening in rate dependent polycrystals*, Acta Metallurgica, **33,** pp. 923-953, 1985.
10. PAN, J., RICE, J. R., *Rate sensitivity of plastic flow and implications for yield-surface vertices*, Int. J. Solid and Struct., **19**, *11*, pp. 973-987, 1983.
11. ZHOU, Y., NEALE, K.W., TOTH, L.S., *A modified model for simulating latent hardening during the plastic deformation of rate-dependent FCC polycrystals*, Int. J. Plasticity, **9**, *8*, pp. 961-978, 1993.
12. HARDER, J., *Crystallographic model for the study of local deformation processes in polycrystals*, Int. J. Plasticity, **15**, *6*, pp. 605-624, 1999.